Supporting Information for

Title: Programmable melt electrowriting to engineer soft connective tissues with prescribed, biomimetic biaxial mechanical properties

Authors: Bahram Mirani[1,2,3,#], Sean O. Mathew[4], Neda Latifi[1,3], Michel R. Labrosse[5,6], Brian G. Amsden[4], Craig A. Simmons[1,2,3,#]

[1]Department of Mechanical & Industrial Engineering, University of Toronto, Toronto, Ontario, Canada, M5S 3G8

[2]Institute of Biomedical Engineering, University of Toronto, Toronto, Ontario, Canada, M5S 3G9

[3]Translational Biology and Engineering Program, Ted Rogers Centre for Heart Research, Toronto, Ontario, Canada, M5G 1M1

[4]Department of Chemical Engineering, Queen's University, Kingston, Ontario, Canada, K7L 3N6

[5]Department of Mechanical Engineering, University of Ottawa, Ottawa, Ontario, Canada, K1N 6N5

[6]Division of Cardiac Surgery, University of Ottawa Heart Institute, Ottawa, Ontario, Canada, K1Y 4W7

[#]Corresponding Authors:

Craig A. Simmons
Translational Biology & Engineering Program, Ted Rogers Centre for Heart Research
University of Toronto
661 University Avenue, 14th Floor
Toronto, Ontario,
Canada, M5G 1M1
Telephone: 416-946-0548
Fax: 416-978-7753
Email: c.simmons@utoronto.ca

Bahram Mirani
Translational Biology & Engineering Program, Ted Rogers Centre for Heart Research
University of Toronto
661 University Avenue, 14th Floor
Toronto, Ontario,
Canada, M5G 1M1
Telephone: 416-978-7365
Email: b.mirani@mail.utoronto.ca

1- Characterization of polycaprolactone (PCL)

PCL was pressure-cast into 1.5-mm thick sheets at 100 °C, a temperature close to what was used in the melt electrowriting (MEW) process. Using a dog-bone-shaped punch with 1.8 mm of width in the narrowest cross-section, PCL sheets were cut (Figure S1A) and used for tensile mechanical testing. Mechanical properties of PCL were determined using a UniVert uniaxial mechanical tester (CellScale, Canada) equipped with a water chamber by applying tensile force while keeping the temperature constant at 37 °C. The resultant stress-strain curve is shown in Figure S1B.

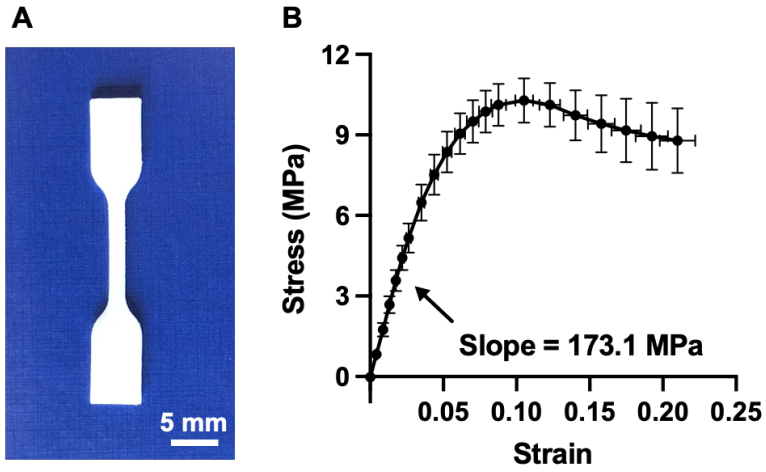

Figure S1. A) Dog-bone-shaped polycaprolactone (PCL) samples used for mechanical characterization using uniaxial loading cycles at 37°C. **B)** The stress-strain relationship for PCL, determined via tensile testing.

2- Mechanical characterization of pediatric porcine PC tissue

Pediatric porcine hearts harvested from animals at 7-8 weeks of age were kindly provided by Dr. Robert Friendship (Ontario Veterinary College, University of Guelph). PC tissues from four donors were cut into 4.5×4.5 mm^2 samples and mounted to a biaxial mechanical tester (BioTester 5000, CellScale, Canada) using a tine sample attachment system (Biorakes with 0.7 mm tine spacing, CellScale, Canada), as shown in Figure S7A. The test procedure and data analysis were similar to that described in the main text for characterizing fibrous scaffolds. Following, tension-strain curves were determined for both circumferential and longitudinal directions of the tissue in equibiaxial loading cycles, as presented in Figure S7B.

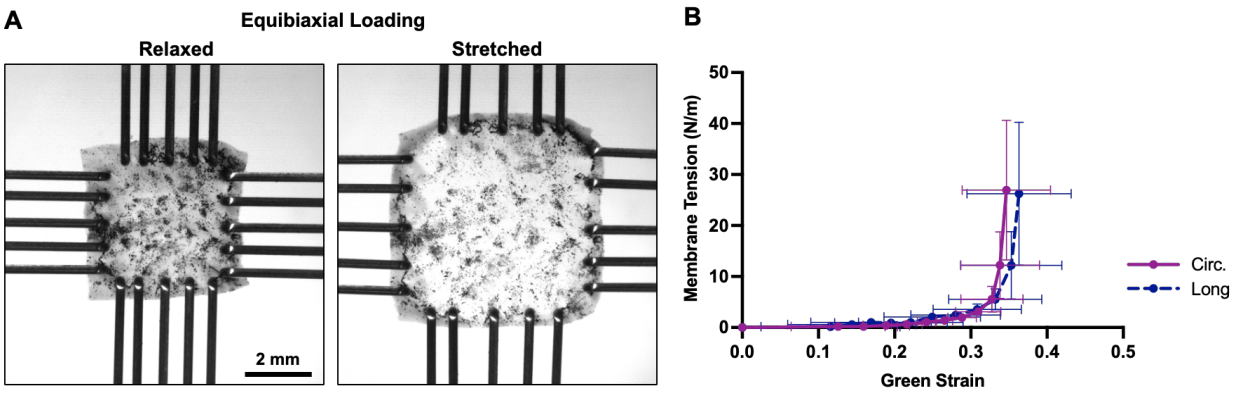

Figure S2. Biaxial mechanical properties of pediatric pericardium tissues using equibiaxial loading cycles. **A)** Tissue in relaxed and equibiaxially stretched conditions. **B)** Tension-strain behaviour of the pericardium tissue in circumferential (Circ.) and longitudinal (Long.) directions, undergoing biaxial tensile test.

3- Optimization of simulated fibrous scaffolds in the computational model

For anisotropic scaffolds, i.e., the aortic valve (AV) and pulmonary valve (PV) conditions, the architecture of the scaffold was defined by the wave amplitude of circumferentially oriented ($Amp_{Circ.}$) and radially oriented ($Amp_{Rad.}$) fibres, the wavelength of circumferentially oriented ($WL_{Circ.}$) and radially oriented fibres ($WL_{Rad.}$), and fibre scaping described below.

$$Spacing_{Circ.} = NWL_{Rad.} \times WL_{Rad.}$$

$$Spacing_{Rad.} = NWL_{Circ.} \times WL_{Circ.}$$

where $Spacing_{circ.}$ is the spacing between circumferentially oriented fibres; $Spacing_{rad.}$ is the spacing between radially oriented fibres; $NWL_{circ.}$ is the number of wavelengths of circumferentially oriented fibres between two adjacent radially oriented fibres; $NWL_{rad.}$ is the number of wavelengths of radially oriented fibres between two adjacent circumferentially oriented fibres. The design matrix for the full factorial design of experiments based on the six architectural variables ($Amp_{circ.}$, $Amp_{rad.}$, $WL_{circ.}$, $WL_{rad.}$, $NWL_{circ.}$, and $NWL_{rad.}$) are described in Table S1.

Table S1. Design matrix for the full factorial design of experiments method to optimize the architecture of the simulated fibrous scaffolds in the computational model for the aortic and pulmonary valve conditions. $Amp_{Circ.}$ and $Amp_{Rad.}$ are the wave amplitude of circumferentially and radially oriented fibres, respectively. $WL_{Circ.}$ and $WL_{Rad.}$ are the wavelength of circumferentially and radially oriented fibres, respectively. $NWL_{circ.}$ is the number of wavelengths of circumferentially oriented fibres between two adjacent radially oriented fibres, and $NWL_{rad.}$ is the number of wavelengths of radially oriented fibres between two adjacent circumferentially oriented fibres.

Computational Conditions	Coded Variables					
	$Amp_{Circ.}$	$Amp_{Rad.}$	$WL_{Circ.}$	$WL_{Rad.}$	$NWL_{Circ.}$	$NWL_{Rad.}$
DOE 1	-1	-1	-1	-1	-1	-1
DOE 2	-1	-1	-1	-1	-1	1
DOE 3	-1	-1	-1	-1	1	-1
DOE 4	-1	-1	-1	-1	1	1
DOE 5	-1	-1	-1	1	-1	-1

DOE 6	-1	-1	-1	1	-1	1
DOE 7	-1	-1	-1	1	1	-1
DOE 8	-1	-1	-1	1	1	1
DOE 9	-1	-1	1	-1	-1	-1
DOE 10	-1	-1	1	-1	-1	1
DOE 11	-1	-1	1	-1	1	-1
DOE 12	-1	-1	1	-1	1	1
DOE 13	-1	-1	1	1	-1	-1
DOE 14	-1	-1	1	1	-1	1
DOE 15	-1	-1	1	1	1	-1
DOE 16	-1	-1	1	1	1	1
DOE 17	-1	1	-1	-1	-1	-1
DOE 18	-1	1	-1	-1	-1	1
DOE 19	-1	1	-1	-1	1	-1
DOE 20	-1	1	-1	-1	1	1
DOE 21	-1	1	-1	1	-1	-1
DOE 22	-1	1	-1	1	-1	1
DOE 23	-1	1	-1	1	1	-1
DOE 24	-1	1	-1	1	1	1
DOE 25	-1	1	1	-1	-1	-1
DOE 26	-1	1	1	-1	-1	1
DOE 27	-1	1	1	-1	1	-1
DOE 28	-1	1	1	-1	1	1
DOE 29	-1	1	1	1	-1	-1
DOE 30	-1	1	1	1	-1	1
DOE 31	-1	1	1	1	1	-1
DOE 32	-1	1	1	1	1	1
DOE 33	1	-1	-1	-1	-1	-1
DOE 34	1	-1	-1	-1	-1	1
DOE 35	1	-1	-1	-1	1	-1
DOE 36	1	-1	-1	-1	1	1
DOE 37	1	-1	-1	1	-1	-1
DOE 38	1	-1	-1	1	-1	1
DOE 39	1	-1	-1	1	1	-1
DOE 40	1	-1	-1	1	1	1
DOE 41	1	-1	1	-1	-1	-1
DOE 42	1	-1	1	-1	-1	1
DOE 43	1	-1	1	-1	1	-1
DOE 44	1	-1	1	-1	1	1
DOE 45	1	-1	1	1	-1	-1
DOE 46	1	-1	1	1	-1	1
DOE 47	1	-1	1	1	1	-1
DOE 48	1	-1	1	1	1	1
DOE 49	1	1	-1	-1	-1	-1

DOE 50	1	1	-1	-1	-1	1
DOE 51	1	1	-1	-1	1	-1
DOE 52	1	1	-1	-1	1	1
DOE 53	1	1	-1	1	-1	-1
DOE 54	1	1	-1	1	-1	1
DOE 55	1	1	-1	1	1	-1
DOE 56	1	1	-1	1	1	1
DOE 57	1	1	1	-1	-1	-1
DOE 58	1	1	1	-1	-1	1
DOE 59	1	1	1	-1	1	-1
DOE 60	1	1	1	-1	1	1
DOE 61	1	1	1	1	-1	-1
DOE 62	1	1	1	1	-1	1
DOE 63	1	1	1	1	1	-1
DOE 64	1	1	1	1	1	1
DOE 65	0	0	0	0	0	0

For isotropic scaffolds, i.e., the pericardium (PC) condition, the architecture of the scaffold in the computational model was defined by wave amplitude (Amp), wavelength (WL), and fibre spacing, described below, in both circumferential and longitudinal directions.

$$Spacing = NWL \times WL$$

where NWL is the number of wavelengths between two adjacent fibres.

Table S2. Design matrix for the full factorial design of experiments method to optimize the architecture of the simulated fibrous scaffolds in the computational model for the pericardium condition. Amp is wave amplitude, WL is wavelength, and NWL is the number of wavelengths between two adjacent fibres.

Computational Conditions	Coded Variables		
	Amp	WL	NWL
DOE 1	-1	-1	-1
DOE 2	-1	-1	1
DOE 3	-1	1	-1
DOE 4	-1	1	1
DOE 5	1	-1	-1
DOE 6	1	-1	1
DOE 7	1	1	-1
DOE 8	1	1	1
DOE 9	0	0	0

Using a least square estimation, model parameters for all factors (amplitude, wavelength, and fibre spacing in both circumferential and radial directions) were calculated (Figure S2) and used to determine the architecture that leads to native tissue mechanics.

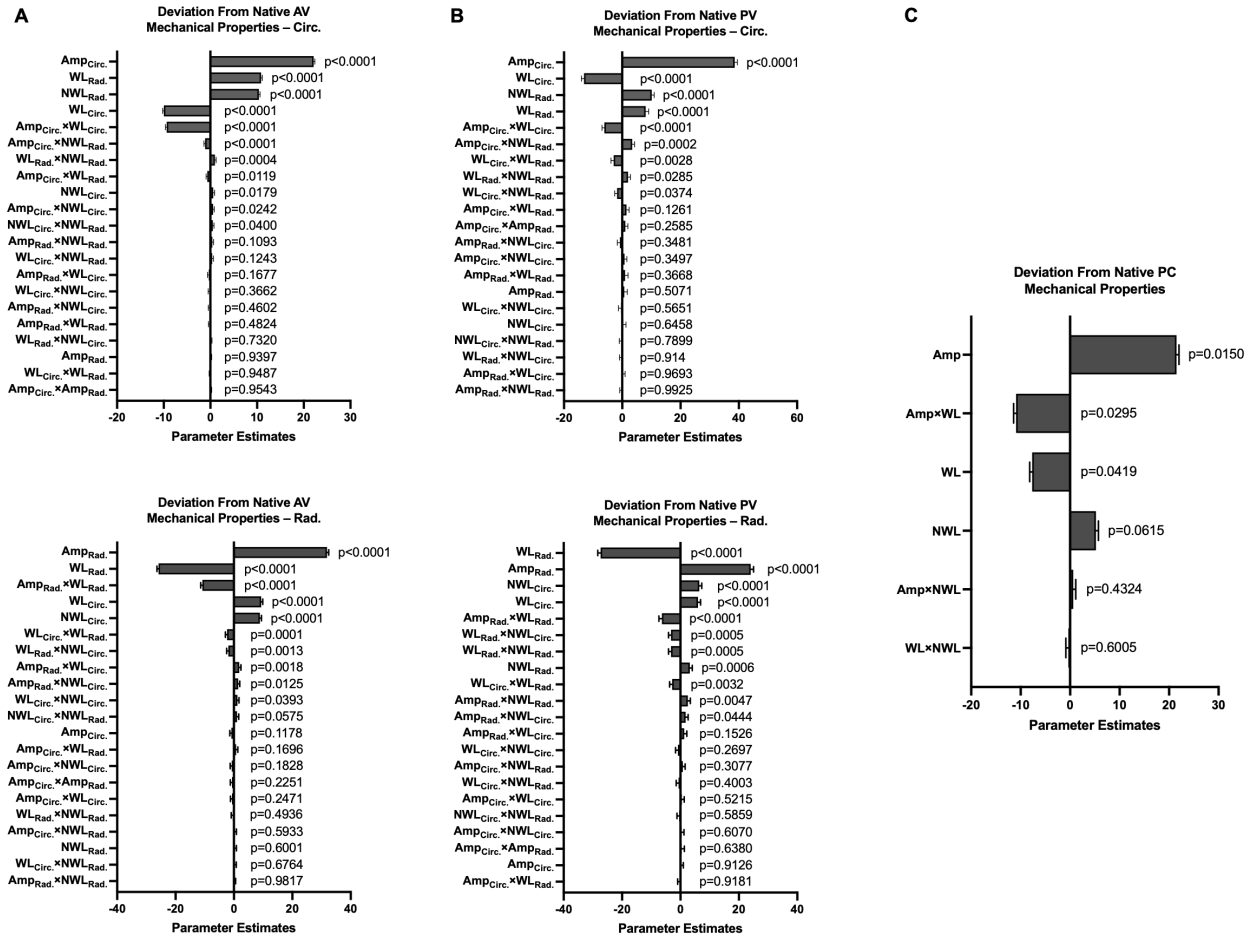

Figure S3. A) Parameter estimate calculated using least square regression to relate fibrous scaffold mechanical properties for aortic valve (AV) and pulmonary valve (PV) conditions (represented by deviation from their native tissue tension-strain behaviour) and scaffold architecture, defined by the wave amplitude of circumferentially oriented ($Amp_{Circ.}$) and radially oriented ($Amp_{Rad.}$) fibres, the wavelength of circumferentially oriented ($WL_{Circ.}$) and radially oriented fibres ($WL_{Rad.}$), $NWL_{Circ.}$ as the number of wavelengths of circumferentially oriented fibres between two adjacent radially oriented fibres, and $NWL_{rad.}$ as the number of wavelengths of radially oriented fibres between two adjacent circumferentially oriented fibres. B) Parameter estimate to relate fibrous scaffold mechanical properties for pericardium (PC) condition and scaffold architecture defined by wave amplitude (Amp), wavelength (WL), and the number of wavelengths between two adjacent fibres (NWL).

4-Single-layer scaffolds composed of sinusoidal fibres printed above the critical translation speed (CTS)

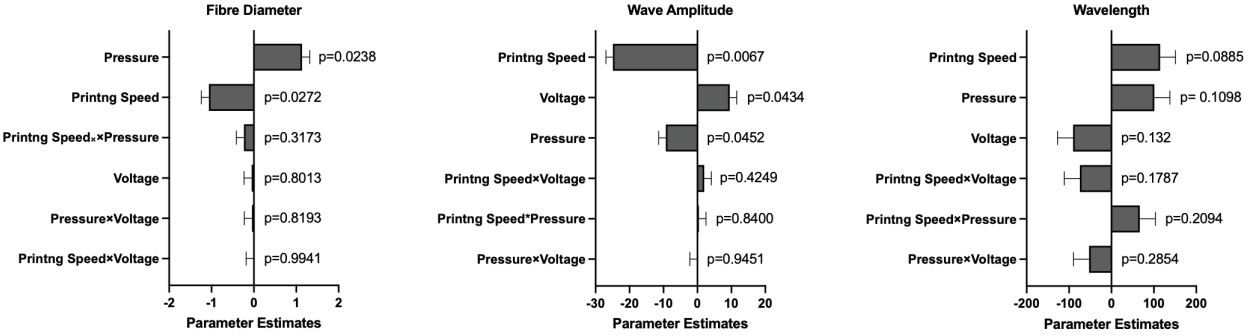

Figure S4. Parameter estimate calculated using least square regression to relate sinusoidal fibre architecture, defined by fibre diameter, wave amplitude, and wavelength to the working parameters of the melt electrowriting (MEW) method,

i.e., printing speed, print-head pressure, and voltage. This estimation was used to determine the MEW parameters for the fabrication of prescribed architectures demonstrated in Figure 2C.

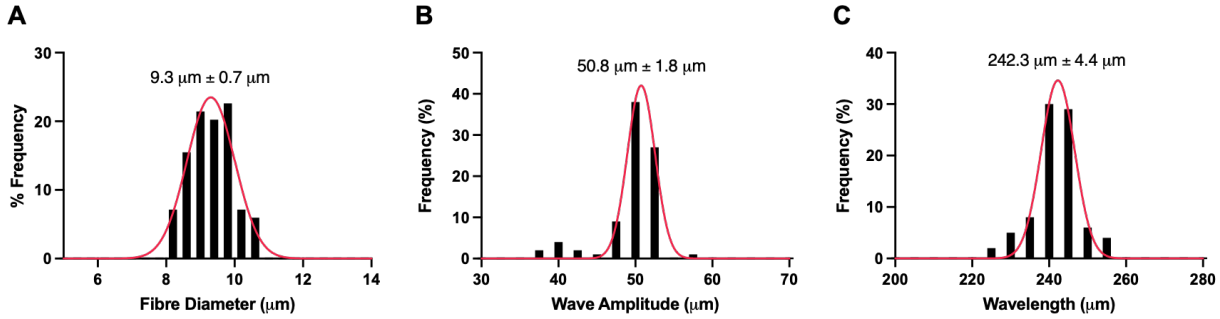

Figure S5. Frequency distribution of fibre diameter (A), wave amplitude (B), and wavelength (C) in a single-layer fibrous scaffold fabricated using melt electrowriting while printing below the critical translation speed. The scaffold refers to what is represented in Figure 2C-i.

5- Multi-layer scaffolds printed above the CTS

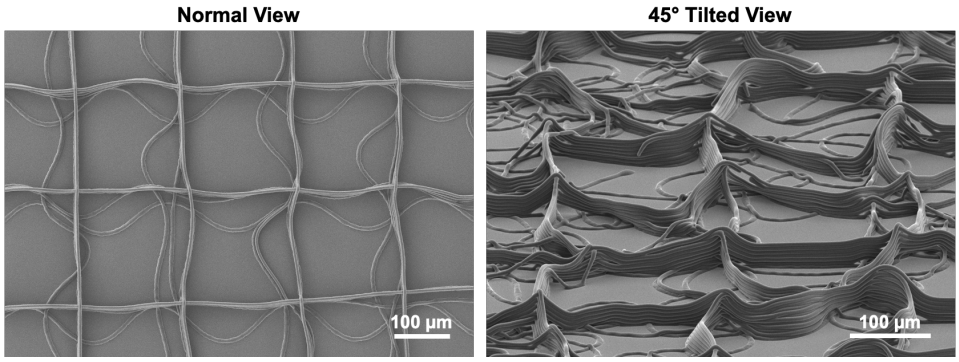

Figure S6. Printing below the critical translation speed did not allow consistent morphology across layers in multilayer scaffolds.

6- Multi-layer scaffolds composed of sinusoidal fibres printed below the CTS

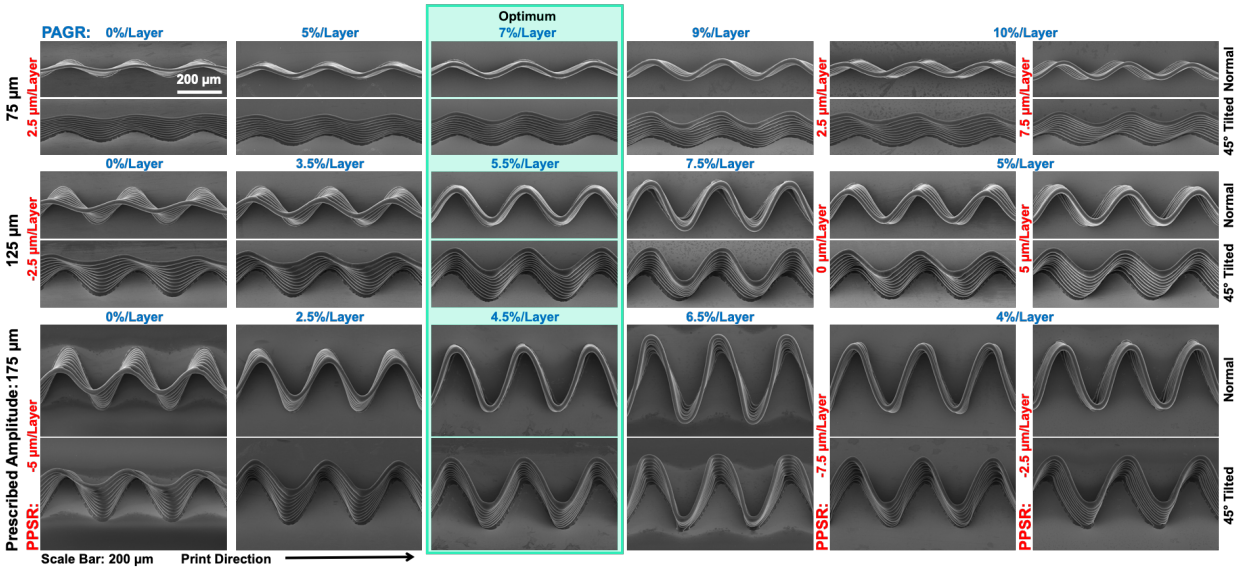

Figure S7. Characterization of print path parameters, i.e., prescribed amplitude growth rate (PAGR) and prescribed phase shift rate (PPSR), in various wave amplitude values, when printing above the critical translation speed on sinusoidal print paths.

7- Experimental optimization of fibrous scaffold

As described in the main text, fibrous scaffolds were optimized using full factorial DOE and parametric modelling via linear regression. The design matrices for these optimizations for AV, PV and PC conditions are shown in tables S3–S5.

Table S3. Design matrix for the full factorial design of experiments method to optimize the architecture of the fibrous scaffolds, fabricated using melt electrowriting, for the aortic valve tissue condition. $Amp_{circ.}$ and $Amp_{rad.}$ are the wave amplitude of circumferentially and radially oriented fibres, respectively.

Experimental Condition	Coded Variables		Actual Variables	
	$Amp_{Circ.\cdot}$	$Amp_{Rad.\cdot}$	$Amp_{Circ.\cdot}$	$Amp_{Rad.\cdot}$
DOE 1	-1	-1	40	90
DOE 2	-1	1	40	150
DOE 3	1	-1	80	90
DOE 4	1	1	80	150
DOE 5 – Centre point	0	0	60	120

Table S4. Design matrix for the full factorial design of experiments method to optimize the architecture of the fibrous scaffolds, fabricated using melt electrowriting, for the pulmonary valve tissue condition. $Amp_{circ.}$ and $Amp_{rad.}$ are the wave amplitude of circumferentially and radially oriented fibres, respectively.

Experimental Condition	Coded Variables		Actual Variables	
	$Amp_{Circ.\cdot}$	$Amp_{Rad.\cdot}$	$Amp_{Circ.\cdot}$	$Amp_{Rad.\cdot}$
DOE 1	-1	-1	70	150
DOE 2	-1	1	70	200
DOE 3	1	-1	130	150
DOE 4	1	1	130	200
DOE 5 – Centre point	0	0	100	175

Table S5. Design matrix for the full factorial design of experiments method to optimize the architecture of the fibrous scaffolds, fabricated using melt electrowriting, for the pericardium tissue condition. Amp is the wave amplitude in both circumferential and longitudinal directions.

Experimental Condition	Coded Variables	Actual Variables
	Amp	Amp
DOE 1	-1	100
DOE 2	1	200
DOE 3 – Centre point	0	150

8- Cell-laden fibrin hydrogel and hybrid fibre-hydrogel constructs

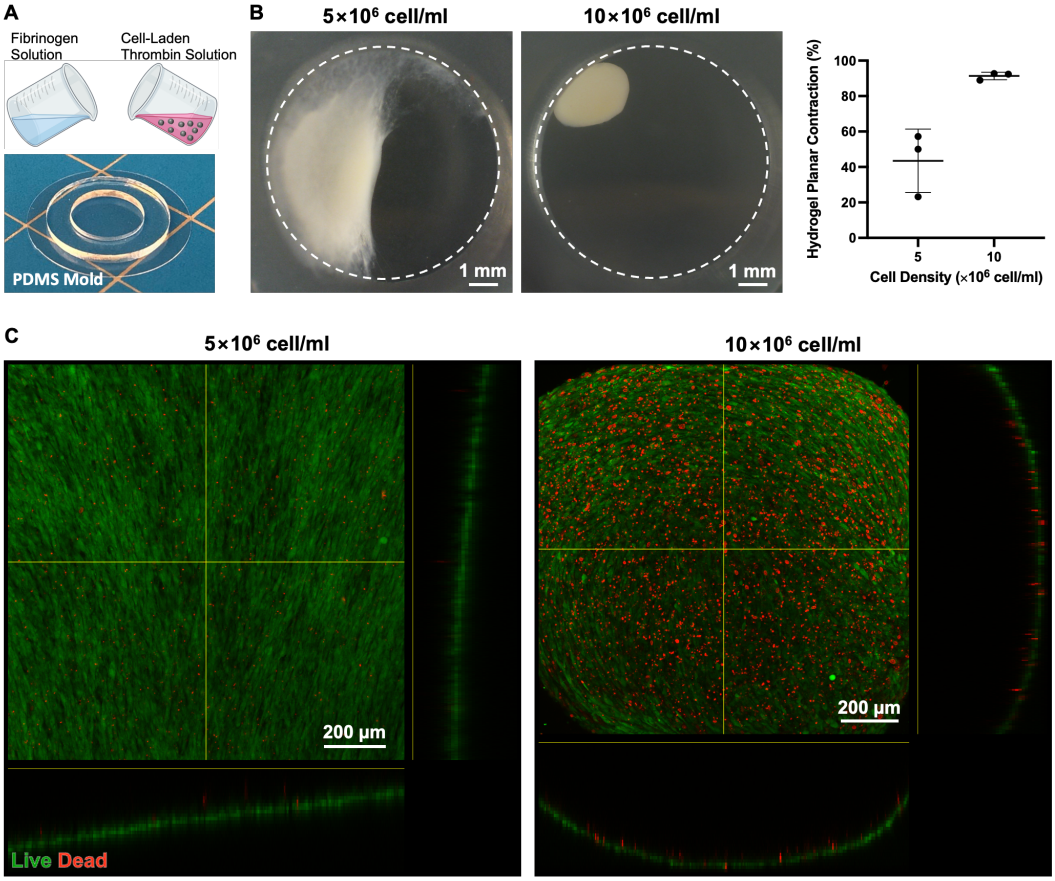

Figure S8. A) Fabrication of cell-laden fibrin hydrogel using a polydimethylsiloxane mold and mixing equal volumes of fibrinogen and cell-laden thrombin solution. **B)** Contraction of cell-laden fibrin hydrogels composed of 5 mg/ml fibrinogen containing 5×10^6 and 10×10^6 cell/ml. C) Cell viability of cell-laden fibrin hydrogels composed of 5 mg/ml fibrinogen containing 5×10^6 and 10×10^6 cell/ml.

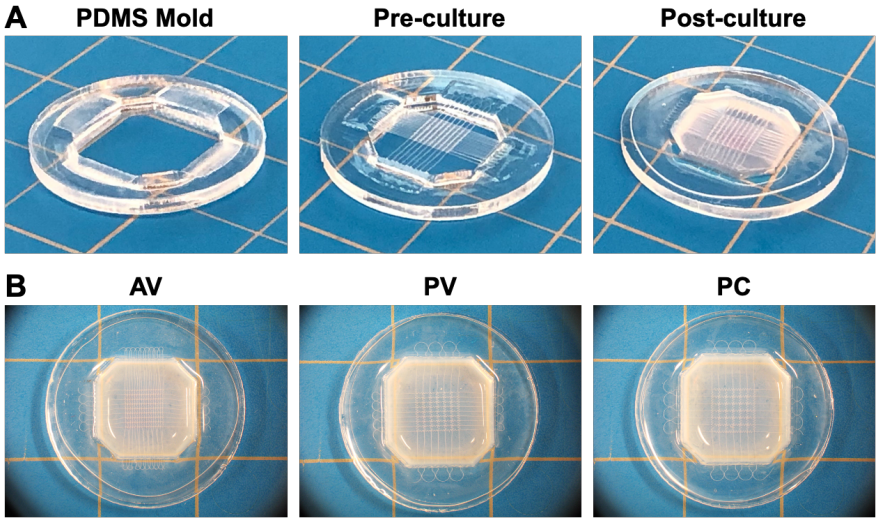

Figure S9. A) Fabrication of hybrid fibre-hydrogel constructs using polydimethylsiloxane molds. **B)** Hybrid constructs fabricated for engineering adult aortic valve (AV), pediatric pulmonary valve (PV) and pediatric pericardium (PC) tissues.

9- Determination of PCL molecular weight and thermal properties

The molar mass dispersity and number average molecular weight (Mn) of PCL were measured using a Waters gel permeation chromatography (GPC) system. The GPC sample solution was prepared at a concentration of 3−10 mg/mL using HPLC grade tetrahydrofuran (THF) and filtered through a 0.2 μm poly(tetrafluoroethylene) syringe filter. Polymer thermal properties, such as glass transition temperature (Tg) and melting point (Tm), were determined using a Mettler-Toledo DSC1 differential scanning calorimeter. The samples were run at a heating and cooling rate of 10 °C/min that was applied over a temperature range program containing two cycles between −100 to 80 °C. The inflection point of the second heating cycle and the minimum of the endothermic curve in the first heating cycle were considered as Tg and Tm, respectively.

10- Temperature and humidity during the MEW process

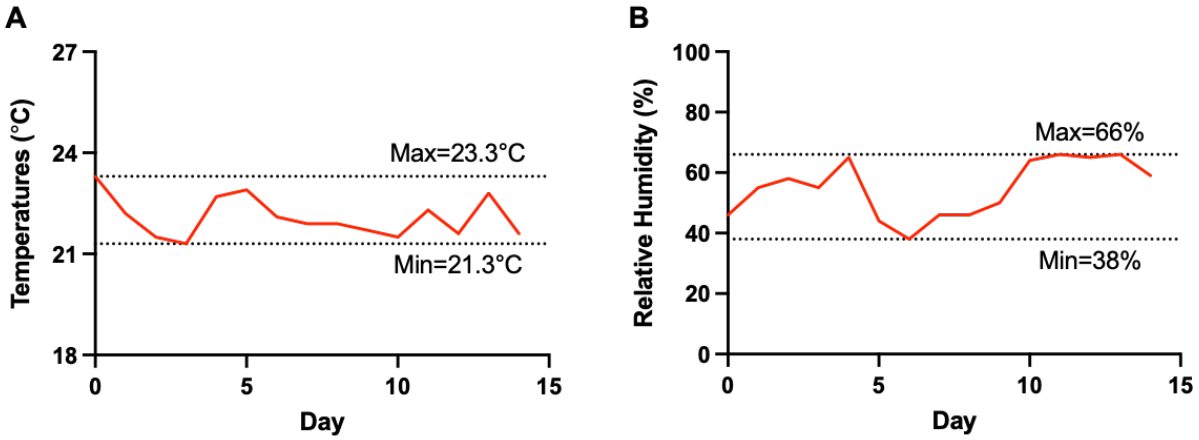

Figure S10. Temperature **(A)** and relative humidity **(B)** were monitored in the melt electrowriting device chamber during 14 days of scaffold fabrication.